Article

Buffeting Characteristics of a Long-Span Cable-Stayed Bridge Crossing a Deep Canyon during Erection: Response Evaluation and Vibration Control

Yichi Zhang [1], Tianyi Zhang [1,*] and Yi Su [2]

[1]   Sichuan Road & Bridge Group Co., Ltd., Chengdu 610041, China; shwayspistachio@gmail.com
[2]   Key Laboratory of New Technology for Construction of Cities in Mountain Area, School of Civil Engineering, Chongqing University, Chongqing 400045, China; windsu888@cqu.edu.cn
*   Correspondence: zty_swjtu@126.com

Abstract: The stiffness of a long-span cable-stayed bridge under construction may be much lower than that observed in service, making it more susceptible to wind effects, especially for a bridge designed using high piers crossing a deep canyon. To study the buffeting characteristics of such cable-stayed bridges under construction, a long-span cable-stayed bridge (the main span is 575 m) is taken as the engineering background. In this study, the buffeting responses and vibration countermeasures at three different construction states were systematically studied using time-domain analysis. It was found that the buffeting response enlarges with an increase in the wind attack angle. The RMS values of the vertical buffeting of the bridge deck end are relatively greater at the maximum double cantilever construction state and maximum single cantilever state. At maximum double cantilever construction state, the traditional wind-resistant cable connecting the bridge deck end to the bridge pile cap significantly reduces the vertical buffeting response, while the suppression effect on lateral and torsional buffeting is limited. When the bridge deck nears completion, wind-resistant cables installed at both cantilever ending in the 'soft connection' method would effectively suppress the vertical, lateral, and torsional buffeting. The suppression effect of cross-arranged wind-resistant cables is superior to that of the parallel arrangement. It is recommended that a reasonable wind-resistant cable layout scheme according to different construction conditions is selected.

Keywords: long-span cable-stayed bridge; construction state; buffeting response evaluation; time-domain analysis; vibration control; wind-resistant cable

1. Introduction

In the atmospheric boundary layer, the oncoming turbulent wind induces flexible structures to undergo random forced vibrations called buffeting. In general, it is impossible to directly destroy the structure. However, for long-span bridges, the prolonged vibration under frequently encountered wind speeds would risk the security of the vehicles and cause discomfort for pedestrians. More seriously, it may cause fatigue damage to the components of the bridge [1–4]. Nowadays, balanced cantilever methods have been widely adopted to construct long-span cable-stayed bridges. Noting that the stiffness of a cable-stayed bridge during erection may be much lower than that in service. The cable-stayed bridge under construction is more susceptible to wind effects [5–7]. Moreover, long-span bridges usually employ the design of high piers to cross deep canyons, resulting in larger buffeting responses.

The theoretical analysis of buffeting responses can adopt the frequency-domain method or time-domain method. Of the two, the frequency-domain method, which depends on the probability statistical concept and pertains to linear structures, was established by Davenport in the 1960s [8–10]. On this basis, the effect of structural motion was considered by introducing the concept of flutter derivative proposed by Scanlan [11–15]. The

flutter derivatives can be used to express the relationship between the structural buffeting response and the aerodynamic self-excited force. Thereafter, many scholars further developed frequency-domain analysis methods. The conventional frequency-domain method is on the basis of the linear hypothesis. Noting that for long-span bridges, the nonlinearity caused by geometric or aeroelastic effects needs to be considered in the buffeting calculation. Therefore, the frequency-domain method is not so suitable for long-span bridges [16]. As an alternative method, the time-domain method would take into account the nonlinearities caused by aerodynamic forces and large deformations. It is critical to transform the aerodynamic force from a spectral form to a time history and to simultaneously calculate the transient aerodynamic force caused by the motion. Baluarte Bridge is a cable-stayed bridge with a mid-span length of 520 m in Mexico. The study on the buffeting response of this bridge showed that the calculation results using the frequency-domain analysis are less than 30% of the full aeroelastic model wind tunnel test results, while the results of time-domain analysis are close to the experimental results [17–19]. Nowadays, the time-domain analysis method has been widely used with the improvement of numerical calculation ability [20–25].

In addition to accurately predicting the buffeting response of the bridge, controlling excessive buffeting responses is a crucial aspect of constructing a cable-stayed bridge to ensure the safety of both personnel and structures [26]. Many researchers have studied countermeasures to suppress the buffeting of long-span cable-stayed bridges. For cable-stayed bridges crossing sea or river with shallow water depth, the installation of temporary piers or steel buttresses under the bridge deck cantilever is widely used to improve the vertical stiffness of the bridge, thereby improving the stability of the bridge [27,28]. It is worth noting that cable-stayed bridges crossing deep canyons are characterized by high piers, and the construction of temporary piers or steel buttresses is not suitable due to high construction costs and poor safety. Moreover, the installation of large mechanical control devices on the bridge deck, such as the tuned mass dampers (TMDs), would decrease the wind-induced vibrations by increasing the damping ratio [29,30]. However, this method has the problems of short installation time, poor economy, and occuping the working space of the bridge deck. Currently, various forms of wind-resistant cables have been adopted to control the excessive buffeting responses of cable-stayed bridges during erection. Among these methods, diagonal wind-resistant cables anchored to the top surface of the pile cap are typically used to mitigate wind-induced responses [31–33]. In addition, the vertical wind-resistant cables anchored to the foundation or ground were also used in the Busan-Geoje Fixed Link Project and the Chishi Bridge during erection [34]. The wind-resistant cables are not sensitive to the topography of the bridge site and are therefore suitable for use in mountain areas. However, when the cantilever length of the bridge deck continues to increase, the length of the wind-resistant cable also increases, resulting in inconvenience during construction.

It is worth noting that the previous studies on the wind-induced vibration of cable-stayed bridges usually focused on plains and coastal areas and often only studied a single construction state. At present, the construction of expressways is gradually expanding to mountain and plateau areas, especially in the mountain areas of southwest China. There are more challenges for the construction of long-span cable-stayed bridges with high piers in complex terrains. However, the research on buffeting response analysis and targeted countermeasures is still insufficient. This paper focuses on the cable-stayed bridge with a high pier design crossing a deep canyon and studies the buffeting characteristics under the representative state throughout the whole construction process. The purpose is to propose a targeted buffeting suppression scheme suitable for the different construction states of cable-stayed bridges in mountain areas to ensure the safety and convenience of bridge construction. To this aim, a long-span cable-stayed bridge with a main span of 575 m crossing a "V" shaped deep canyon is taken as the engineering background. The time-domain FEM method is used to calculate the buffeting response under the different construction states, which include maximum double-cantilever construction state, single-

cantilever mid-term construction state, and maximum single-cantilever construction state. The suppression effects of various forms of wind-resistant cables on the buffeting response are also systematically investigated.

2. Time-Domain Method for the Buffeting Response Evaluation of Long-Span Bridges

The present study adopts the time-domain method to analyze the buffeting response of the long-span cable-stayed bridge, which takes into account the nonlinear factors that the frequency-domain method cannot include. The calculation procedures of this method are as follows. First, the discrete three-dimensional turbulent flow field around the bridge is simulated according to the meteorological data and terrain at the bridge site. Second, the aerodynamic coefficients of the cross-sections of the bridge deck and tower are identified to calculate the time histories of the aerodynamic forces acting on the structure. Finally, the finite element method (FEM) is used to analyze buffeting responses through the step-by-step time series analysis. It is assumed that the oncoming flow is orthogonal to the bridge deck in the analysis. The theoretical method of bridge buffeting analysis is briefly introduced as follows.

2.1. Three-Dimensional Turbulent Wind Field Simulation

The turbulent wind can be decomposed in three different directions, including longitudinal direction (u), lateral direction (v), and vertical direction (w). Furthermore, three-dimensional turbulent wind field can be simplified into three orthogonal one-dimensional turbulent flow fields if the correlation between the wind fields is not considered. Thus, the three-dimensional wind fields can be expressed in the Cartesian coordinate system as:

$$\begin{cases} U = \overline{U}(z) + u(x,z,t) \\ \quad v = v(x,z,t) \\ \quad w = w(x,z,t) \end{cases} \tag{1}$$

where U is the longitudinal velocity of the oncoming wind; $\overline{U}(z)$ is the mean longitudinal velocity; x and z are the longitudinal and lateral coordinates, respectively; u, v, and w are longitudinal, lateral, and vertical fluctuating velocities; and t is the time parameter.

To simulate the wind field around a bridge, the field can be discretized using a three-dimensional wind field with discrete finite points in a certain area. Then, the time history of the velocity of each discrete point can be simulated by superimposing the mean and fluctuating velocities of the oncoming wind. In the atmospheric boundary layer, the mean longitudinal velocity varies with the height from the ground, which can be expressed by exponential law or logarithmic law. Moreover, the fluctuating wind speeds in three directions would be calculated by the harmony superposition method. For this method, it is critical to generate random process samples through the superposition of random trigonometric functions according to the given wind speed spectrum and correlation function.

2.2. Wind Loads Simulation

- Aerostatic force

The aerostatic force acting on a structure is expressed using Formula (2),

$$\begin{aligned} F_D &= \tfrac{1}{2}\rho U^2 C_D(\alpha_0) D \\ F_L &= \tfrac{1}{2}\rho U^2 C_L(\alpha_0) B \\ F_M &= \tfrac{1}{2}\rho U^2 C_M(\alpha_0) B^2 \end{aligned} \tag{2}$$

where ρ is the air density; α_0 is the average wind attack angle of oncoming flow; C_D, C_L, and C_M are drag, lift, and lift moment coefficients; and D and B are height and width of bridge deck.

- Buffeting force

Based on the quasi-steady theory, the aerodynamic force under fluctuating wind can be expressed as

$$
\begin{aligned}
L_b(t) &= \tfrac{1}{2}\rho U^2 B[C_L(\alpha_0)\chi_{Lu}\tfrac{u(t)}{U} + (C_L'(\alpha_0) + C_D(\alpha_0))\chi_{Lw}\tfrac{w(t)}{U}] \\
D_b(t) &= \tfrac{1}{2}\rho U^2 B[2C_D(\alpha_0)\chi_{Du}\tfrac{u(t)}{U} + C_D'(\alpha_0)\chi_{Dw}\tfrac{w(t)}{U}] \\
M_b(t) &= \tfrac{1}{2}\rho U^2 B^2[2C_M(\alpha_0)\chi_{Mu}\tfrac{u(t)}{U} + C_M'(\alpha_0)\chi_{Mw}\tfrac{w(t)}{U}]
\end{aligned}
\tag{3}
$$

where C_D', C_L', and C_M' are the slopes of the curves of the aerostatic coefficients, which are identified using sectional model wind tunnel tests or numerical simulation, and χ_{Du}, χ_{Dw}, χ_{Lu}, χ_{Lw}, χ_{Mu}, and χ_{Mw} are aerodynamic admittances of drag, lift, and lift moment.

- Aerodynamic self-excited force

According to the theoretical expression proposed by Scanlan, the aerodynamic lift force L_{ae}, drag force D_{ae}, and lift moment M_{ae} per unit length can be written as

$$
\begin{aligned}
L_{ae} &= \tfrac{1}{2}\rho U^2(2B)\left[KH_1^*\tfrac{\dot{h}}{U} + KH_2^*\tfrac{B\dot{\alpha}}{U} + K^2H_3^*\alpha + K^2H_4^*\tfrac{h}{B} + KH_5^*\tfrac{\dot{p}}{U} + K^2H_6^*\tfrac{p}{B}\right] \\
D_{ae} &= \tfrac{1}{2}\rho U^2(2B)\left[KP_1^*\tfrac{\dot{p}}{U} + KP_2^*\tfrac{B\dot{\alpha}}{U} + K^2P_3^*\alpha + K^2P_4^*\tfrac{p}{B} + KP_5^*\tfrac{\dot{h}}{U} + K^2P_6^*\tfrac{h}{B}\right] \\
M_{ae} &= \tfrac{1}{2}\rho U^2(2B)\left[KA_1^*\tfrac{p\dot{h}}{U} + KA_2^*\tfrac{B\dot{\alpha}}{U} + K^2A_3^*\alpha + K^2A_4^*\tfrac{h}{B} + KA_5^*\tfrac{\dot{p}}{U} + K^2A_6^*\tfrac{p}{B}\right]
\end{aligned}
\tag{4}
$$

where h represents vertical position; α represents torsional position; p is horizontal displacement; and H_i^*, P_i^*, and A_i^* $(i = 1, 2, 3 \cdots, 6)$ are aerodynamic derivatives, which only related to the cross-section shape. In this paper, the aerodynamic self-excited force is calculated using the method proposed by Ding [35].

3. Research Background and Numerical Setup

3.1. Research Background

A cable-stayed bridge crossing a typical deep 'V'-shaped canyon was taken as a research engineering background. Figure 1 illustrates the bridge's general arrangement. This bridge is located in the mountainous area of Southwest China. The main span of the bridge is 575 m, and its total length is 1089 m. As shown in Figure 2, the bridge deck is an opening steel-concrete composite cross-section with two 'I'-shaped longitudinal edge girders. It is 38.0 m in width and 3.0 m in height. Two 'L'-shaped deflectors are installed at both edges of the cross-section to suppress vortex-induced vibration. The two concrete towers have heights of 261.0 m and 217.0 m, respectively. The relative height difference between the bridge deck and the ground is about 330 m. The bridge is constructed using the traditional cantilever assembly method. Figure 3 shows three typical states during erection, including maximum double cantilever construction state, mid-term single cantilever construction state, and maximum single cantilever construction state. The maximum double cantilever state is the state when the cantilever length of the main beam is the largest before the connection between the main beam and the side pier. When the bridge deck is installed except for the closure section, it is in the maximum single cantilever construction state, and the bridge deck has the maximum cantilever length. The mid-term single cantilever construction state is the intermediate state of the transition from the maximum double cantilever state to the maximum single cantilever state. In the present study, these three typical construction states were considered.
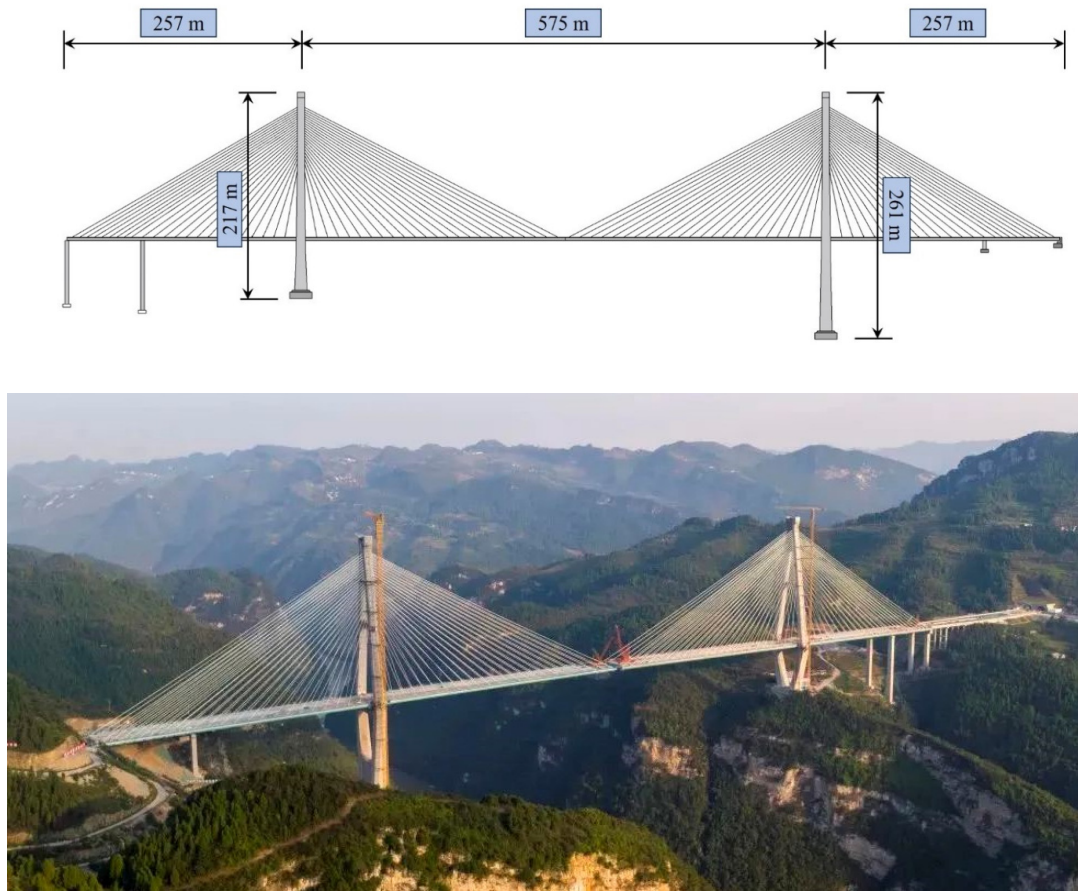
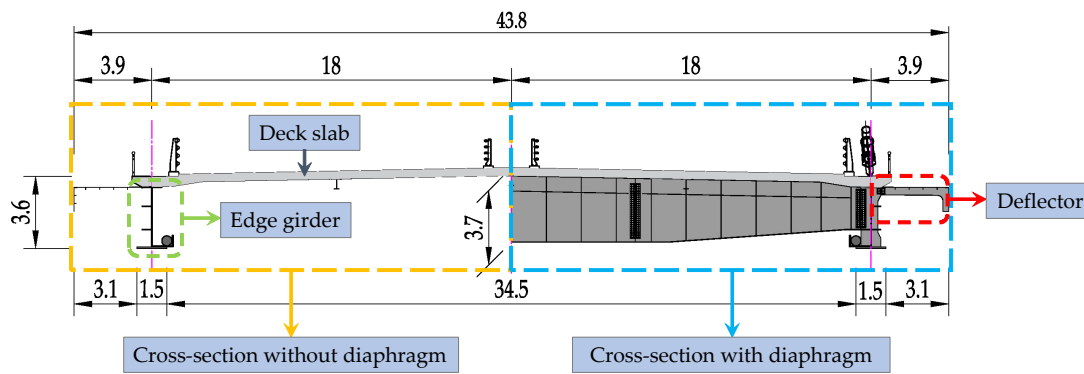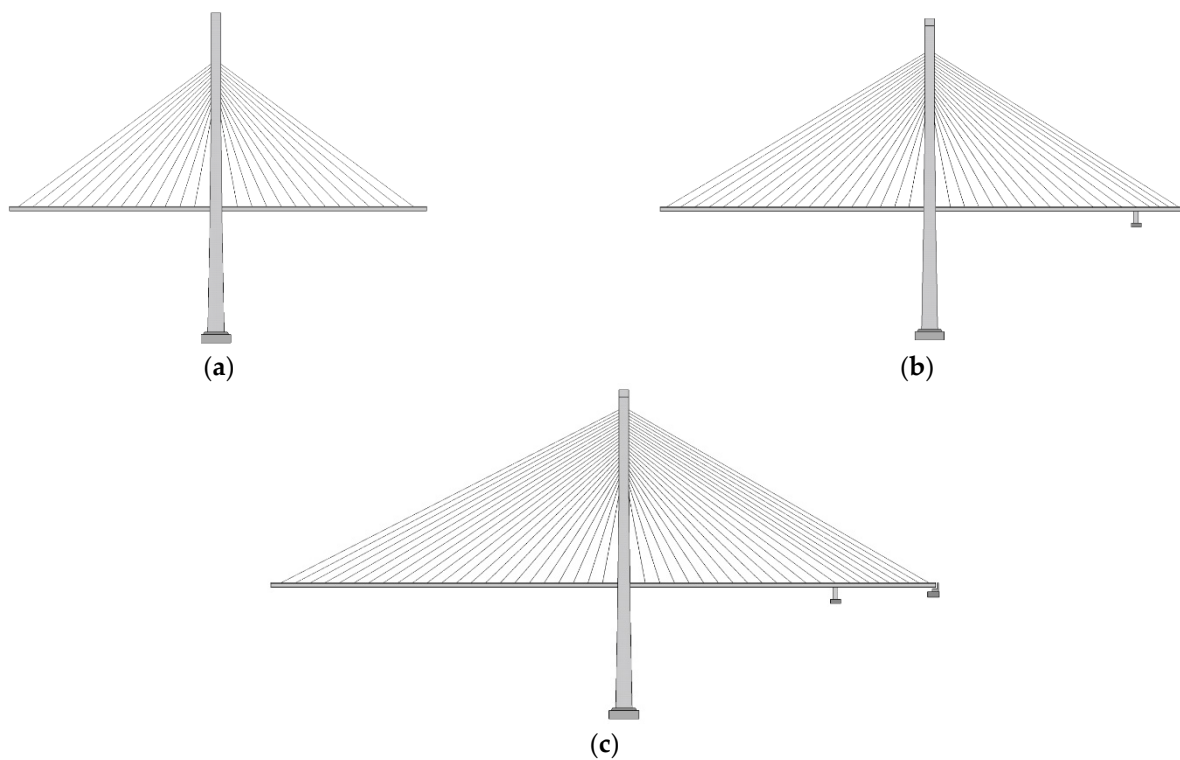**Figure 1.** The general arrangement and photo of the bridge.

Figure 2. The cross-sections of the bridge main beam (unit: m).

Figure 3. Schematic diagrams of the bridge at three construction states. (**a**) maximum double cantilever construction state; (**b**) mid-term single cantilever construction state; (**c**) maximum single cantilever construction state.
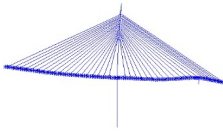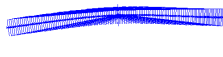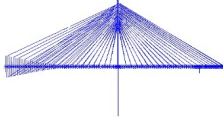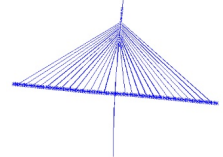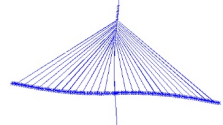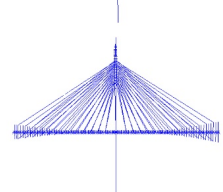
3.2. Dynamic Characteristics

The FEM software ANSYS 15.0 was used to construct the three-dimensional model and solve the dynamic characteristics results. In the model, the sliding bearing of the cable-stayed bridge was fixed during erection. The frequencies and mode shapes of typical vibration modes of the bridge deck in three different states are listed in Table 1.

Table 1. Dynamic characteristics of the bridge deck at different construction states.

Construction State	Order	Vibration Mode	Frequency (Hz)	Mode Shape
maximum double cantilever state	1	Vertical bending–symmetric	0.1297	
	2	Lateral bending–symmetric	0.2322	
	10	Torsion–symmetric	1.2387	

Table 1. *Cont.*

Construction State	Order	Vibration Mode	Frequency (Hz)	Mode Shape
single cantilever medium-term state	1	Vertical bending–symmetric	0.2491	
	2	Lateral bending–symmetric	0.2858	
	9	Torsion–symmetric	1.0193	
maximum single cantilever state	1	Lateral bending of tower	0.1297	
	2	Lateral bending–symmetric	0.2322	
	4	Vertical bending–symmetric	0.4535	
	10	Torsion–symmetric	1.2387	

3.3. Setup of the Buffeting Response Calculation

- Wind field simulation results

Based on the topographical features, the design mean velocity of the bridge deck height was calculated to be 31.4 m/s during erection using the Chinese wind-resistant design specifications for highway bridges [36]. The surface roughness coefficient α_0 and surface roughness height z_0 were selected to be 0.22 and 0.3 m. The three-dimensional wind field simulation used the Kaimal wind spectrum recommended by Chinese specifications. The power spectrum of the longitudinal fluctuating velocity at the height z is expressed as

$$\frac{nS_u(n)}{(u^*)^2} = \frac{200f}{(1+50f)^{5/3}} \tag{5}$$

The wind power spectrum of vertical fluctuating velocity is written as

$$\frac{nS_\omega(n)}{(u^*)^2} = \frac{6f}{(1+4f)^2} \tag{6}$$

where $S_u(n)$ is the power spectral density function of longitudinal fluctuating velocity; $S_\omega(n)$ is the power spectral density function of vertical fluctuating velocity; n is the frequency of wind; and $f = \frac{nz}{U(z)}$ is the Moning coordinate.

A total of 42 discrete wind simulation points were set along the height direction of the bridge tower. A total of 28, 38, and 48 wind simulation points were set along the bridge deck at the maximal double cantilever construction state, mid-term single cantilever construction state, and maximal single cantilever construction state, respectively. The fluctuating wind time interval was set to 0.0625 s during the simulation. Figure 4 shows the longitudinal and vertical fluctuating velocity time history results of the simulated point of the bridge deck end at the maximum single cantilever state. Figure 5 shows the target and simulated wind spectrums of longitudinal and vertical velocities. The results indicate that the fluctuating velocity of the oncoming wind agrees well with the target spectrum, indicating that the three-dimensional wind field is accurately simulated.

- Determination of aerodynamic coefficients
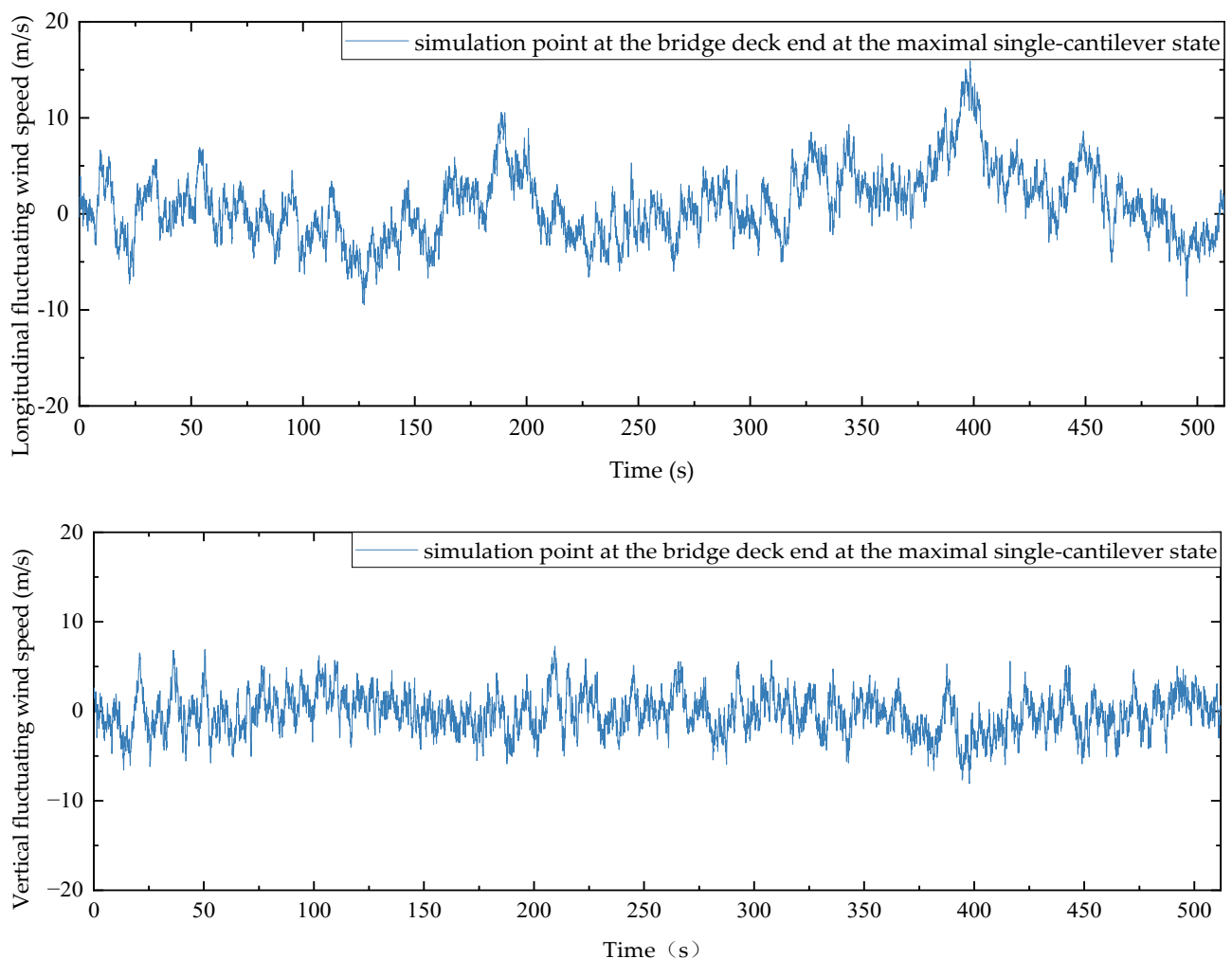
Figure 4. Velocity time history of simulation point at bridge deck end at the maximum single cantilever state.

In this study, the aerodynamic coefficients during erection were obtained through sectional model wind tunnel tests carried out at Tongji University. The identified aerodynamic coefficients are shown in Table 2. The aerodynamic coefficients of the tower were calculated by the CFD method. The aerodynamic admittances were set to 1 to simplify the calculation.
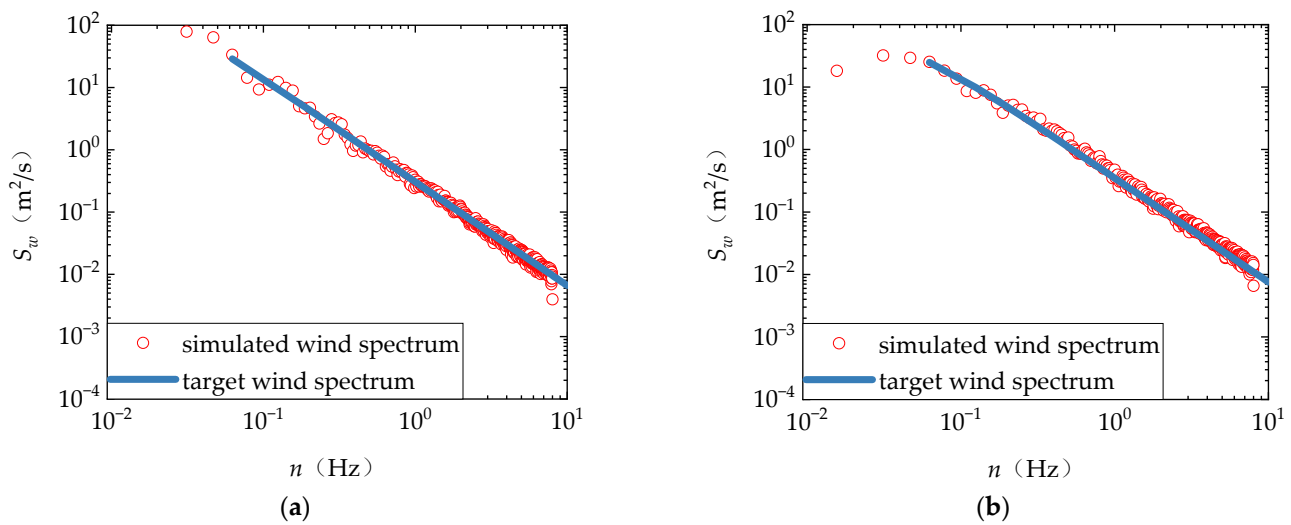
Figure 5. Wind spectrum of simulation point at the bridge deck end at the maximum single cantilever state. (**a**) Longitudinal direction; (**b**) vertical direction.

- Parameters in the time-domain analysis

Table 2. The aerodynamic coefficients of the bridge deck during erection.

Attack Angle	Drag Coefficient C_H	$dC_H/d\alpha$	Lift Coefficient C_V	$dC_V/d\alpha$	Lift Moment Coefficient C_M	$dC_M/d\alpha$
−3°	1.540	−5.133	−0.319	3.644	0.019	0.467
0°	1.414	0.898	−0.062	6.122	0.044	0.408
+3°	1.684	10.340	0.327	8.536	0.050	−0.213

The time-domain analysis in the present study was based on the APDL module in the ANSYS 15.0 FEM software. The calculation time step was 0.125 s in the simulation. In order to ensure the accuracy of the further spectrum analysis results, the number of sampling floating points in the spectrum calculation should be an integer exponential multiple of 2. In addition, through the trial calculation, it can be seen that the root mean square (RMS) value of the structural buffeting response tends to be stable after the calculation time is about 400 s. Therefore, the total simulation time was set to 512 s. Rayleigh damping was adopted to simulate the damping ratio, and the damping ratio was set to 1.0%, according to the Chinese specifications. The windward area of the stay cable is much smaller than that of the bridge deck and tower, the aerodynamic force has limited influence on the calculation results. Thus, the effect of vortex shedding on the stay cable was not considered in the calculation. To fully consider the nonlinearity characteristics of the structure, the gravity and mean aerodynamic forces were initially applied to the model and considered as the first state in the dynamic simulation.

4. Buffeting Responses in Three Different Construction States

The buffeting responses under three wind attack angles (−3°, 0°, and +3°) at different construction states, including maximum double cantilever state, mid-term single cantilever construction state, and maximum single cantilever state, were systematically calculated. Table 3 lists the mean displacement and the RMS induced by the wind effect at the bridge material positions. The displacement time histories at 0° wind attack angle are illustrated in Figure 6.
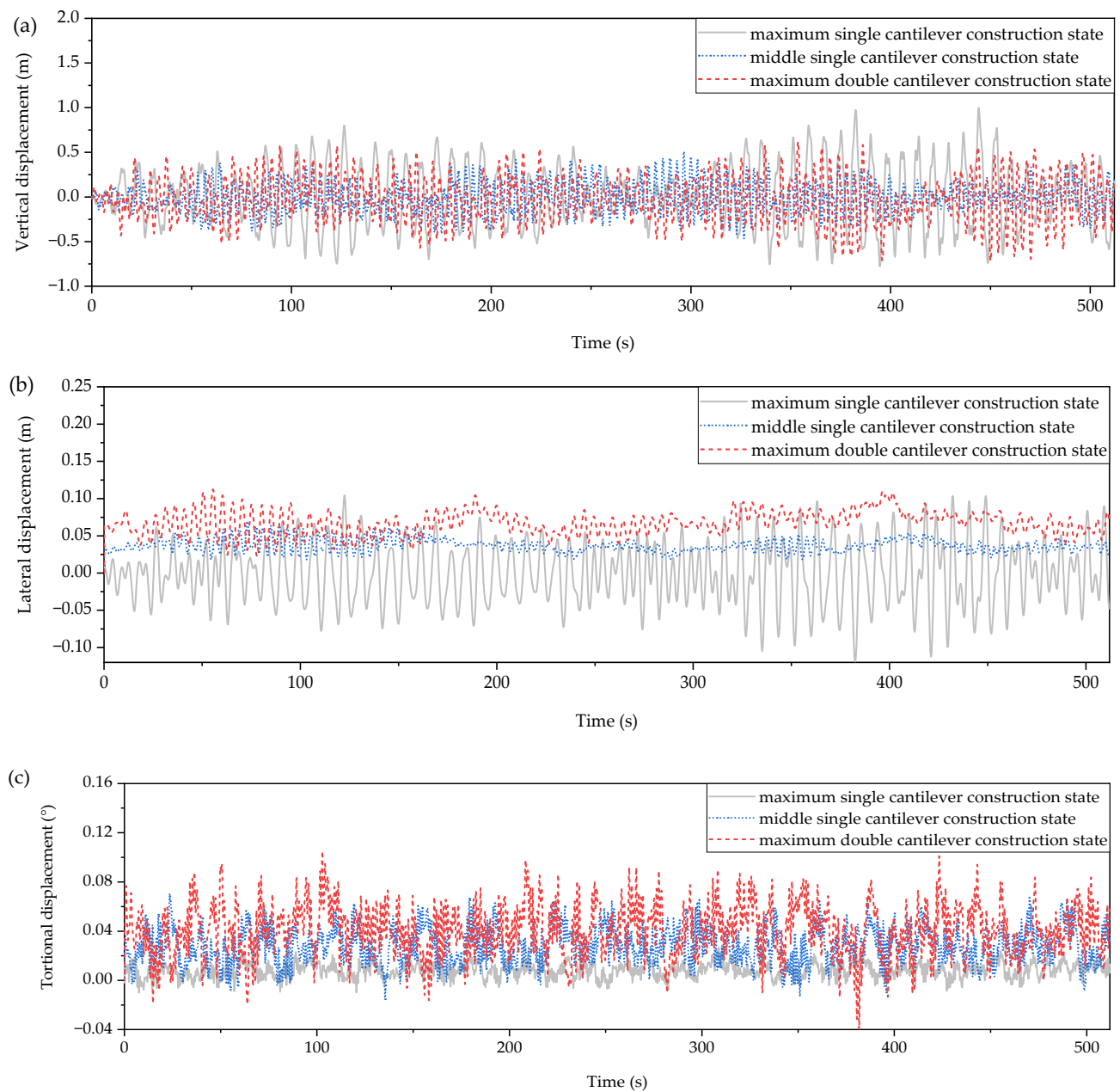
Figure 6. Displacement time histories of the end of the bridge deck cantilever at three construction states at 0° wind attack angle.

It can be seen that the buffeting response at the wind attack angle of +3° is significantly larger than that at the wind attack angles of −3° and 0°, which contributed to the larger slopes of the curves of the aerostatic coefficients. In the following section, the buffeting performance of the bridge at three construction states is investigated based on the simulation at 0° wind attack angle. It is shown that the lateral mean displacements of the bridge deck are significantly greater than the vertical mean displacement at two single cantilever construction states. The vertical RMS value of buffeting responses of the bridge deck cantilever end is largest at the maximum double cantilever state, reaching 0.3390 m. And it is close to the RMS value at the top of the bridge tower. This may indicate that the bridge deck vertical buffeting at the maximum double cantilever construction state mainly relies on the lateral bending of the bridge tower. While the bridge deck vertical displacements at the other two construction states may be participated by bridge deck vibration modes. The RMS values of the lateral and vertical buffeting responses are the largest at the

maximum double cantilever state, reaching 0.0402 m and 0.3390 m, respectively. Moreover, the torsional buffeting response is the largest at the maximum single cantilever state, and the RMS value at the end of the bridge deck cantilever is 0.0205°.

Table 3. The mean displacements and RMS at main positions at three different states.

State	Attack Angle	Position	Longitudinal (m)		Vertical (m)		Lateral (m)		Torsional (°)	
			Mean	RMS	Mean	RMS	Mean	RMS	Mean	RMS
Maximum double cantilever state	−3°	Deck end	/	/	0.0136	0.2538	−0.0014	0.0291	0.0028	0.0069
		Tower top	0.0280	0.2665	/	/	0.0033	0.0041	−0.0019	0.0077
	0°	Deck end	/	/	0.0075	0.3390	−0.0001	0.0402	0.0082	0.0058
		Tower top	0.0121	0.3554	/	/	0.0029	0.0027	−0.0012	0.0104
	+3°	Deck end	/	/	−0.0021	0.4324	0.0016	0.0638	0.0098	0.0052
		Tower top	−0.0127	0.4525	/	/	0.0043	0.0063	−0.0009	0.0182
Medium single cantilever state	−3°	Deck end	/	/	−0.0488	0.1152	0.0398	0.0142	0.0132	0.0170
		Tower top	−0.0140	0.0417	/	/	0.0123	0.0046	0.0027	0.0022
	0°	Deck end	/	/	−0.0113	0.1674	0.0372	0.0087	0.0282	0.0143
		Tower top	−0.0030	0.0610	/	/	0.0119	0.0030	0.0016	0.0013
	+3°	Deck end	/	/	0.0458	0.2293	0.0434	0.0232	0.0331	0.0123
		Tower top	0.0137	0.0839	/	/	0.0135	0.0085	0.0019	0.0023
Maximum single cantilever state	−3°	Deck end	/	/	−0.0863	0.1837	0.0732	0.0325	0.0179	0.0244
		Tower top	−0.0232	0.0588	/	/	0.0151	0.0064	0.0036	0.0030
	0°	Deck end	/	/	−0.0290	0.2561	0.0675	0.0156	0.0409	0.0205
		Tower top	−0.0077	0.0824	/	/	0.01438	0.0032	0.00191	0.00161
	+3°	Deck end	/	/	0.0592	0.3386	0.0773	0.0401	0.0513	0.0182
		Tower top	0.0161	0.1093	/	/	0.0163	0.0086	0.0020	0.0029

To further study the buffeting characteristics at three construction states, the spectrums of the buffeting displacement response of the bridge deck cantilever end at 0° wind attack angle were calculated using FFT, as illustrated in Figure 7. For lateral and torsional buffeting responses, the peak point of the displacement response spectrum is at the natural frequency point, which verifies the correctness of the bridge buffeting response analysis program. It can be seen that, due to the high pier design for the bridge crossing the 'V'-shaped canyon in the mountainous area, the vibration induced by the lateral bending and torsion of the tower dominates the buffeting of the bridge deck at the double cantilever construction state. The vibration caused by the bridge tower is mainly located in a low-frequency region. At single cantilever states, the vibration frequency of the bridge deck increased, in which the vertical buffeting response has multi-order higher frequency participation, especially at the maximum single cantilever state. Meanwhile, the lateral and torsional buffeting responses are dominated by the first-order mode.
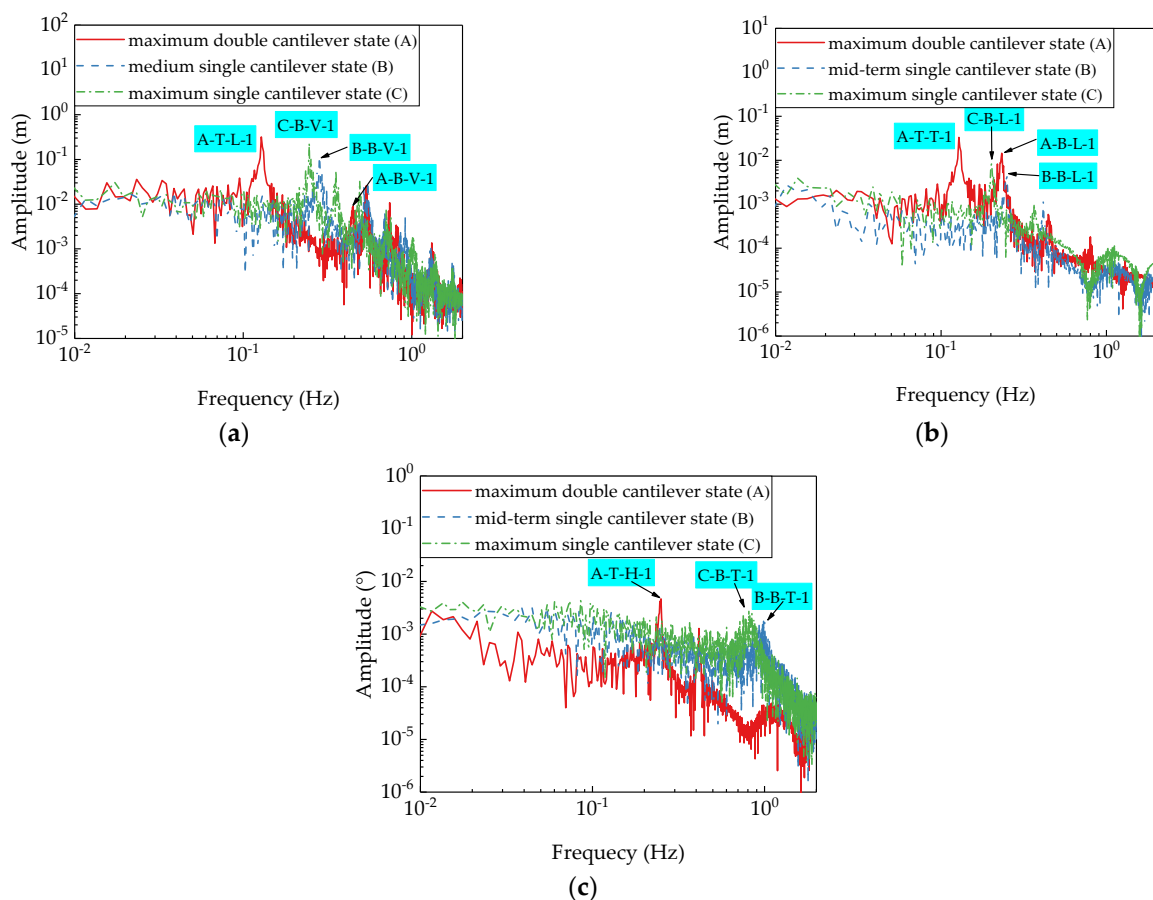
Figure 7. Spectrum of buffeting response of bridge deck end at three construction states, in which A, B, and C represent construction state, respectively; T and B represent tower and bridge, respectively; V, L, and T represent vertical, lateral, and tortional mode, respectively. (**a**) Spectrum of vertical buffeting response at bridge deck end; (**b**) spectrum of lateral buffeting response at bridge deck end; (**c**) spectrum of torsional buffeting response at bridge deck end.

5. Suppression Effect of Wind-Resistant Cables on Buffeting Response

To suppress the effect of buffeting response on cable-stayed bridges during erection, many bridges have been set up with vibration countermeasures. Among them, temporary support piers, TMDs, or various forms of wind-resistant cables are commonly used. Since long-span cable-stayed bridges in mountainous areas usually cross deep canyons, the bridge deck is usually hundreds of meters away from the bottom of the valley, making it difficult to install temporary support piers. In addition, the TMD device is expensive and cannot be recycled. In this investigation, according to the characteristics of long-span cable-stayed bridges crossing deep canyons located in mountainous areas, a variety of buffeting countermeasures based on wind-resistant cables were designed.

As shown in Figure 8a,b, four wind-resistant cables are installed symmetrically at both bridge deck ends at maximum double cantilever state. Two ends of the cable are fixed to the anchorage point of the bridge deck and the top surface of the pile cap, respectively. Considering the reduction in the demolition and installation work of the wind-resistant cables, the arrangement of wind-resistant cable at the single cantilever mid-term state is the same as that at the maximum double cantilever state in this study. Figure 8e,f show that the connection positions between the wind-resistant cables and the bridge deck are located at three-quarters of the bridge deck cantilever length at the maximum single cantilever state. Due to the connection between the bridge deck of the side span and the auxiliary pier, the wind-resistant cables are only set on the mid-span side at the two single cantilever construction states. In addition, considering the short duration of the maximum single

cantilever stage, the 'soft connection' method proposed by Hu, Yang, Li, and Wang [37], as illustrated in Figure 8g,h, is introduced to suppress the buffeting response, consequently avoiding the installation of long wind-resistant cables. The edge girder is a vital force component in the composite bridge deck cross-section, and it needs to bear the large tension of the stay cable. Thus, it usually has great strength in the structural design. Similarly to the stay cable, the anchorage points of the wind-resistant cable are set on the longitudinal edge girder. A total of 120 Φ7 mm hot-dip galvanized steel wires which have the characteristics of good toughness and strong reliability are selected for the wind-resistant cables, and the area of a single cable is 4618.14 mm^2. The pre-tension of each wind-resistant cable is set to be 3 kN. The suppression effects of both parallel and crossed wind-resistant cables are investigated at each construction state.
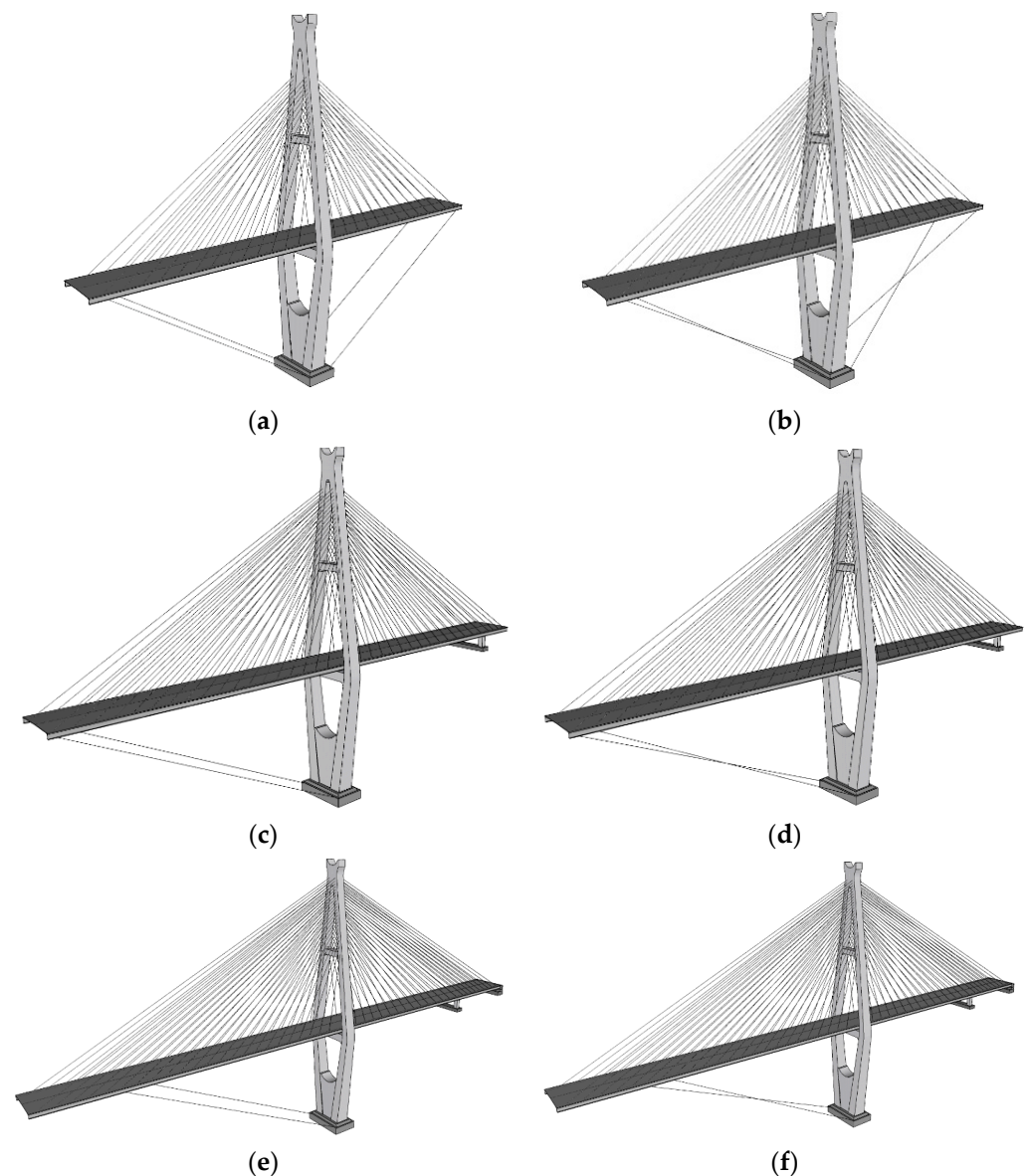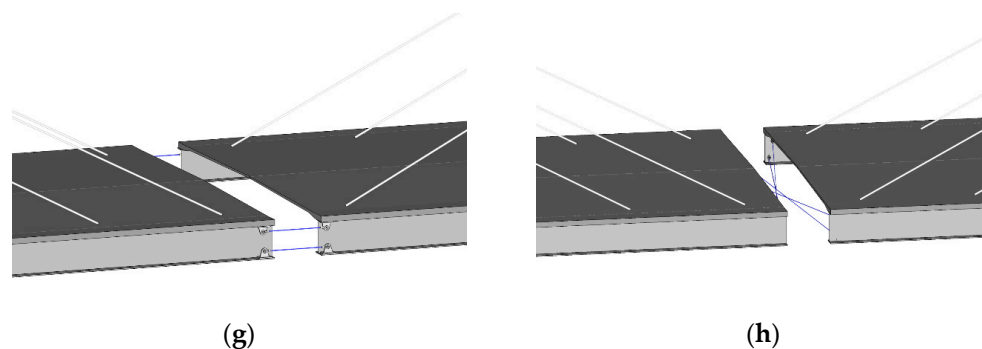

(**a**)　　　　　　　　　　　　　　　(**b**)

(**c**)　　　　　　　　　　　　　　　(**d**)

(**e**)　　　　　　　　　　　　　　　(**f**)

Figure 8. *Cont.*

(**g**)   (**h**)

Figure 8. Design scheme of wind-resistant cables during erection. (**a**) Parallel arrangement at maximum double cantilever state; (**b**) cross arrangement at maximum double cantilever state; (**c**) parallel arrangement at mid-term single cantilever state; (**d**) cross arrangement at mid-term single cantilever state; (**e**) parallel arrangement at maximum single cantilever state; (**f**) cross arrangement at maximum single cantilever state; (**g**) parallel arrangement in 'soft connection' method; (**h**) cross arrangement in 'soft connection' method.

The frequencies of typical bridge deck vibration modes with and without wind-resistant cables are shown in Figure 9. It can be found that the frequencies of the first-order torsion and lateral bending modes can be improved with the installation of traditional wind-resistant cables at the maximum double cantilever state. Compared with the original construction state, the lateral bending and torsion frequencies are increased by 9.5% and 3.9% with the wind-resistant cables, respectively. The installation of the cross-arranged wind-resistant cables in the 'soft connection' method at the maximum single cantilever state can significantly increase the lateral bending frequency and slightly raise the vertical bending and torsion frequencies. The wind-resistant cables have a limited increase in the vibration frequency at other construction conditions, which indicates that installing the wind-resistant cables cannot significantly increase the structural stiffness.

The buffeting time-domain method was adopted to study the suppression effects of buffeting countermeasures. The calculation results in Figure 10 show that, with the symmetrical installation of the four wind-resistant cables at both bridge deck ends at the maximum double cantilever state, the vertical buffeting response of the bridge deck and the lateral bending of the tower are significantly reduced and the vibration reduction rate can reach 55.3%, indicating that this wind-resistant cable arrangement can effectively control the tower lateral bending and the bridge deck vertical buffeting during this construction state. Moreover, with the installation of this countermeasure, the decreased rate of lateral buffeting response is about 20%, and the suppression effect of torsional buffeting response is only within 10%. The bridge deck transforms to the mid-term single cantilever construction state when the bridge deck is connected to the auxiliary pier. The overall stiffness of the bridge is significantly improved, and the buffeting response is remarkably reduced. The application of the traditional wind-resistant cable only has a certain effect on the bridge deck vertical buffeting response and the tower lateral bending buffeting response in cases (c) and (d), and the suppression effect in other directions is not obvious. As the bridge deck cantilever continues to extend, the buffeting response obviously improves. Similarly to the mid-term single cantilever state, the traditional wind-resistant cables have a limited effect on the buffeting at the maximum single cantilever construction state, while the wind-resistant cables in the 'soft connection' method can significantly reduce the buffeting response. Moreover, the suppression effect of cross-connected wind-resistant cables is greater than that of parallel-connected cables. Using cross-connected wind-resistant cables, the reduction rates of vertical, lateral, and torsional buffeting responses of the bridge deck end are 35.6%, 39.3%, and 8.5%, respectively, and the lateral response of the tower top reduces by 27.0%.
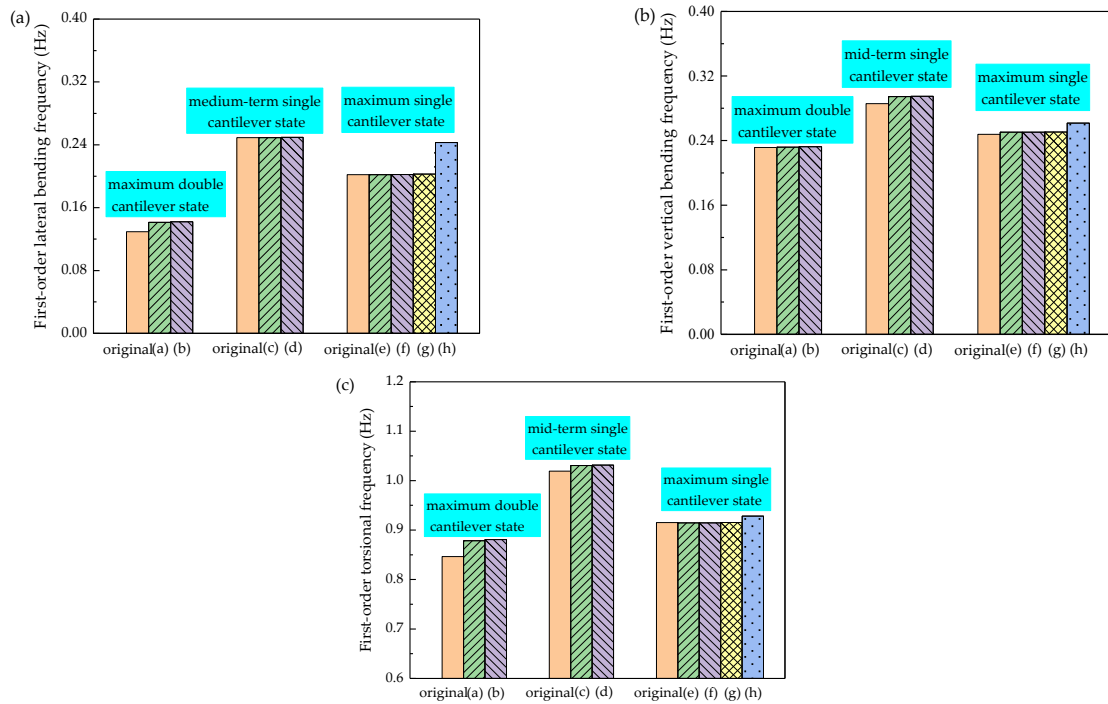
Figure 9. Frequencies of typical vibration modes of bridge deck with and without wind-resistant cables. The lowercase letters in the horizontal axis represent the wind-resistant cable arrangement shown in Figure 8; (**a**) First-order lateral bending frequency (Hz); (**b**) First-order vertical bending frequency (Hz); (**c**) First-order torsional frequency (Hz).
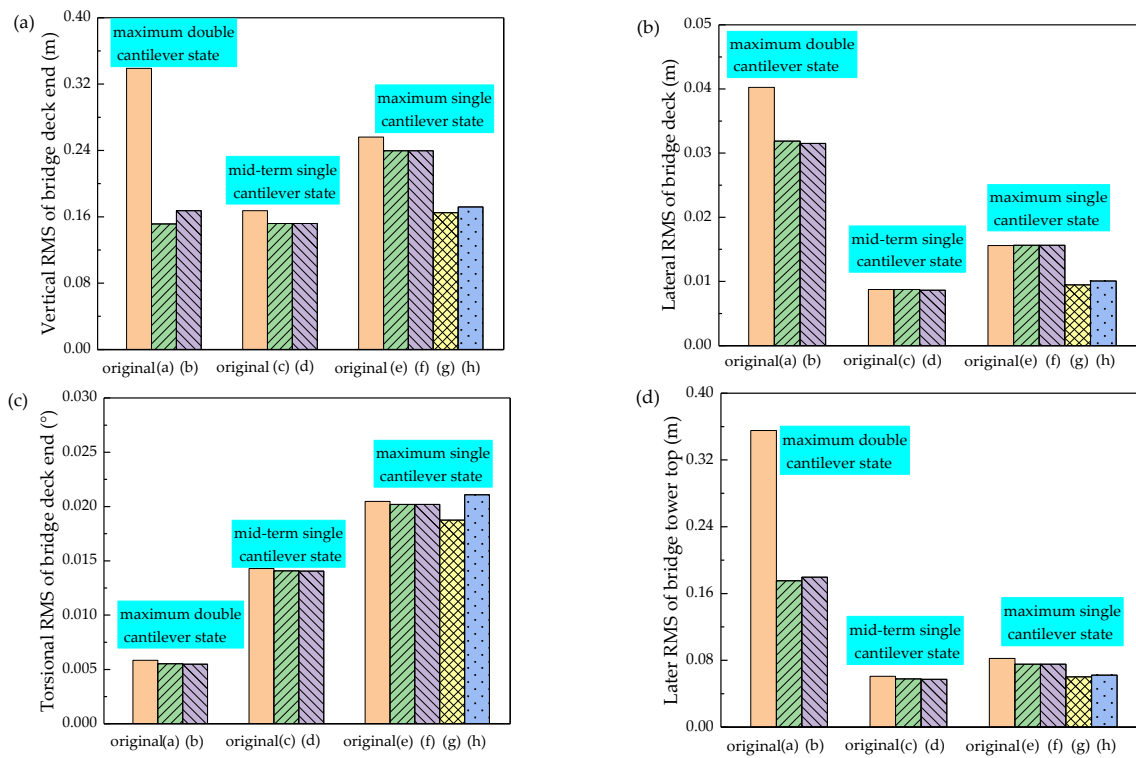
Figure 10. Buffeting responses of the material positions with the wind-resistant cables. The lowercase letters in the horizontal axis represent the wind-resistant cable arrangement shown in Figure 8; (**a**) Vertical RMS of bridge deck end (m); (**b**) Laterla RMS of bridge deck (m); (**c**) Torsional RMS of bridge deck end (°); (**d**) Later RMS of bridge tower top (m).

Based on the above calculation results, for the long-span cable-stayed bridges crossing canyons, reasonably installing wind-resistant cables would effectively decrease the buffeting response during bridge construction. The symmetrical installation of the traditional wind-resistant cables connected to the pile cap effectively reduces the buffeting response at the double cantilever construction state. When the side span connects to the auxiliary pier, the increase in the overall stiffness of the bridge will greatly reduce the buffeting response. The buffeting of the bridge deck end is most significant at maximum single cantilever state, and it is effectively suppressed by installing cross-arranged wind-resistant cables in the 'soft connection' method.

6. Conclusions

A typical long-span cable-stayed bridge was taken into account as the research background to systematically investigate the buffeting characteristics and propose economical vibration countermeasures for long-span cable-stayed bridges crossing deep canyons during erection. The time-domain analysis method was adopted to calculate the buffeting responses at three representative construction states. The main conclusions are as follows.

The results showed that the buffeting response at the wind attack angle of $+3°$ is significantly larger than that at the wind attack angle of $-3°$ or $0°$ due to the larger slopes of the curves of aerostatic coefficients. Driven by the lateral bending of the bridge tower, the bridge deck vertical buffeting response is the largest at the maximum double cantilever construction state. Under the design mean velocity (31.4 m/s), the vertical buffeting displacement RMS value at $0°$ attack angle reaches 0.3390 m. The overall stiffness of the bridge would be increased by connecting the bridge deck to the side pier, significantly reducing buffeting responses. At the maximum single cantilever construction state, the bridge deck cantilever is the longest, and the vertical buffeting displacement RMS value at $0°$ attack angle is 53.0% higher than that at the mid-term single cantilever state.

The traditional wind-resistant cables would greatly reduce the bridge deck vertical buffeting response at the maximum double cantilever construction state. The RMS value of the vertical displacement is reduced by 55.3%. The suppression effects on the lateral and torsional buffetings are limited, and the vibration reduction rate is less than 20%. Moreover, the traditional wind-resistant cable has no obvious suppression effect at the mid-term single cantilever construction state and the maximum single cantilever construction state, and the decreased rates are all not greater than 12%. When the bridge deck is nearing completion, the wind-resistant cables installed using the 'soft connection' method can significantly reduce buffeting responses. Using cross-connected wind-resistant cables, the decreasing rates of vertical, lateral, and torsional buffeting responses of the bridge deck end are 35.6%, 39.3%, and 8.5%, respectively.

It is recommended that a reasonable wind-resistant cable layout scheme according to different construction conditions is selected. In the future, the accuracy of buffeting response calculation will be further verified using wind tunnel tests or field measurements. The method of suppressing the buffeting response by changing the aerodynamic shape of the bridge needs to be investigated.

Author Contributions: Conceptualization, Y.Z. and T.Z.; software, Y.Z.; validation, Y.Z., T.Z. and Y.S.; formal analysis, T.Z.; investigation, Y.Z., T.Z. and Y.S.; writing—original draft preparation, Y.Z.; writing—review and editing, T.Z. and Y.S.; funding acquisition, Y.S. All authors have read and agreed to the published version of the manuscript.

Data Availability Statement: The data presented in this study are available on request from the corresponding author. The data are not publicly available due to reasons of confidentiality.

Conflicts of Interest: Authors Yichi Zhang and Tianyi Zhang were employed by the company Sichuan Road & Bridge Group Co., Ltd. The remaining author declares that the research was conducted in the

absence of any commercial or financial relationships that could be construed as a potential conflict of interest.

References

1. Tao, T.; Wang, H.; Yao, C.; He, X. Parametric Sensitivity Analysis on the Buffeting Control of a Long-Span Triple-Tower Suspension Bridge with MTMD. *Appl. Sci.* **2017**, *7*, 395. [CrossRef]
2. Lystad, T.M.; Fenerci, A.; Øiseth, O. Buffeting response of long-span bridges considering uncertain turbulence parameters using the environmental contour method. *Eng. Struct.* **2020**, *213*, 110575. [CrossRef]
3. Xin, J.; Zhou, C.; Jiang, Y.; Tang, Q.; Yang, X.; Zhou, J. A signal recovery method for bridge monitoring system using TVFEMD and encoder-decoder aided LSTM. *Measurement* **2023**, *214*, 112797. [CrossRef]
4. Zhu, S.; Li, Y.; Yang, Y.; Ju, N. Stochastic Buffeting Analysis of Uncertain Long-Span Bridge Deck with an Optimized Method. *Buildings* **2022**, *12*, 632. [CrossRef]
5. Ma, C.; Duan, Q.; Li, Q.; Liao, H.; Tao, Q. Aerodynamic characteristics of a long-span cable-stayed bridge under construction. *Eng. Struct.* **2019**, *184*, 232–246. [CrossRef]
6. Yan, L.; Ren, L.; He, X.; Lu, S.; Guo, H.; Wu, T. Strong Wind Characteristics and Buffeting Response of a Cable-Stayed Bridge under Construction. *Sensors* **2020**, *20*, 1228. [CrossRef] [PubMed]
7. Zan, S.J.; Tanaka, H.; Yamada, H.; Wardlaw, R.L. Parametric investigation of wind-induced cable-stayed bridge motion using an aeroelastic model. *J. Wind Eng. Ind. Aerodyn.* **1989**, *32*, 161–169. [CrossRef]
8. Davenport, A.G. The spectrum of horizontal gustiness near the ground in high winds. *Q. J. R. Meteorol. Soc.* **1961**, *87*, 194–211. [CrossRef]
9. Davenport, A.G. The response of slender, line-like structures to a gusty wind. *Proc. Inst. Civ. Eng.* **1962**, *23*, 389–408. [CrossRef]
10. Davenport, A.G. The application of statistical concepts to the wind loading of structures. *Proc. Inst. Civ. Eng.* **1961**, *19*, 449–472. [CrossRef]
11. Scanlan, R.H. The action of flexible bridges under wind, II: Buffeting theory. *J. Sound Vib.* **1978**, *60*, 201–211. [CrossRef]
12. Scanlan, R.H. Interpreting Aeroelastic Models of Cable—Stayed Bridges. *Eng. Mech.* **1987**, *113*, 555–575. [CrossRef]
13. Scanlan, R.H.; Jones, N. Aeroelastic Analysis of Cable—Stayed Bridges. *J. Struct. Eng.* **1990**, *116*, 279–297. [CrossRef]
14. Yang, Y.; Li, M.; Ma, C.; Li, S. Experimental investigation on the unsteady lift of an airfoil in a sinusoidal streamwise gust. *Phys. Fluids* **2017**, *29*, 051703. [CrossRef]
15. Li, M.; Yang, Y.; Li, M.; Liao, H. Direct measurement of the Sears function in turbulent flow. *J. Fluid Mech.* **2018**, *847*, 768–785. [CrossRef]
16. Su, C.; Fan, X.; He, T. Wind-induced vibration analysis of a cable-stayed bridge during erection by a modified time-domain method. *J. Sound Vib.* **2007**, *303*, 330–342. [CrossRef]
17. King, J.P.C.; Gomez, R.; Pozos-Estrada, A.; Sánchez-García, R. Experimental and analytical evaluation of the aeroelastic behavior of the Baluarte bridge. In Proceedings of the 13th International Conference on Wind Engineering, Amsterdam, The Netherlands, 10–15 July 2011.
18. Pozos-Estrada, A.; Flores, R.; Gómez, R. Parametric Study of Stay Cables of a Bridge Under Simulated Spatially Correlated Turbulent Wind. *Lat. Am. J. Solids Struct.* **2016**, *13*, 1450–1463. [CrossRef]
19. Landero, H.H. Simulation of non-homogeneous wind processes. In *Comparison between Numerical and Experimental Model of a Bridge*; The University of Western Ontario: London, ON, Canada, 2022.
20. Wu, T.; Kareem, A. Modeling hysteretic nonlinear behavior of bridge aerodynamics via cellular automata nested neural network. *J. Wind Eng. Ind. Aerodyn.* **2011**, *99*, 378–388. [CrossRef]
21. Chen, X.; Kareem, A. Nonlinear response analysis of long-span bridges under turbulent winds. *J. Wind Eng. Ind. Aerodyn.* **2001**, *89*, 1335–1350. [CrossRef]
22. Li, Y.; Kareem, A. Simulation of Multivariate Random Processes: Hybrid DFT and Digital Filtering Approach. *J. Eng. Mech.* **1993**, *119*, 1078–1098. [CrossRef]
23. Diana, G.; Rocchi, D.; Argentini, T. An experimental validation of a band superposition model of the aerodynamic forces acting on multi-box deck sections. *J. Wind Eng. Ind. Aerodyn.* **2013**, *113*, 40–58. [CrossRef]
24. Wang, H.; Li, A.; Hu, R. Comparison of Ambient Vibration Response of the Runyang Suspension Bridge under Skew Winds with Time-Domain Numerical Predictions. *J. Bridge Eng.* **2011**, *16*, 513–526. [CrossRef]
25. Diana, G.; Resta, F.; Rocchi, D. A new numerical approach to reproduce bridge aerodynamic non-linearities in time domain. *J. Wind Eng. Ind. Aerodyn.* **2008**, *96*, 1871–1884. [CrossRef]
26. Yan, L.; Ren, L.; He, X.; Li, Y.; Du, B.; Zhong, R. Experimental Study of Buffeting Control of Pingtang Bridge during Construction. *J. Bridge Eng.* **2020**, *25*, 05020004. [CrossRef]
27. Ge, Y.; Yang, Y.; Zhao, L.; Cao, F. Study of Wind Resistant Stability of Main Navigable Span Bridge of Shanghai Changjiang River Bridge. *World Bridges* **2020**, *S1*, 62–72.
28. Su, Z.; Peng, J. Buffeting-Restraining Measures for Long Span Cable-Stayed Bridges at the Longest Double Cantilever Construction Stage. *Highw. Eng.* **2018**, *43*, 146–151.
29. Shen, Z.; Hu, Z.; Li, J.; Xue, X.; Gao, G. Controlling the Modal Coupled Buffeting Response of the Long Span Dense-frequency Cable-stayed Bridge by MDTMD. *China J. Highw. Transp.* **2019**, *32*, 135–149.

30. Zapateiro, M.; Pozo, F. *Advances on Analysis and Control of Vibrations: Theory and Applications*; IntechOpen: London, UK, 2012.

31. Moir, G.; Edmonds, C.; Walser, P.; Romberg, M. Construction Engineering of Phu My Cable-Stayed Bridge, Vietnam. *Struct. Eng. Int.* **2010**, *20*, 331–337. [CrossRef]

32. Kim, B.-J.; Lee, S.-H.; Kim, H.-K. Mokpo Bridge: New Landmark in Mokpo City. *Struct. Eng. Int.* **2012**, *22*, 29–31. [CrossRef]

33. Svensson, H.S. *Cable-Stayed Bridges: 40 Years of Experience Worldwide*; Ernst & Sohn: Berlin, Germany, 2012.

34. Kim, Y.M.; Jeong, S.K.; Joo, S.J. Wind-resistant measures of the Busan~Geoje Fixed Link Bridges during construction. In Proceedings of the 18th Congress of IABSE, Seoul, Republic of Korea, 19–21 September 2012; IABSE: Seoul, Republic of Korea, 2012; pp. 660–667.

35. Ding, Q. *Refinement of Coupled Flutter and Buffeting Analysis for Long-Span Bridges*; Tongji University: Shanghai, China, 2001.

36. Ministry of Transport of the People's Republic of China. *Wind-Resistant Design Specification for Highway Bridges*; China Communications Press: Beijing, China, 2018.

37. Hu, X.; Yang, S.; Li, Y.; Wang, Q. Study of Buffeting Response and Suppression Measures for Composite Girder Cable Stayed Bridge in Longest Cantilever State During Construction. *Bridge Constr.* **2021**, *51*, 21–27.